Site Change Detection for RADIUS using Thermophysical Algebraic Invariants *

N. Nandhakumar[†], **J.D. Michel**[†], **D.G. Arnold**[†‡], **V. Velten**[‡], and **G.A. Tsihrintzis**[†]
[†] Dept of Electrical Engineering, Univ. of Virginia, Charlottesville, VA 22903
[‡] Wright Laboratory - WL/AARA, WPAFB, OH 45433-7001

ABSTRACT

Research on the formulation of invariant features for model-based object recognition has mostly been concerned with geometric constructs either of the object or in the imaging process. We describe a new method that identifies invariant features computed from long wave infrared (LWIR) imagery. These features are called thermophysical invariants and depend primarily on the material composition of the object. Features are defined that are functions of only the thermophysical properties of the imaged materials. A physics-based model is derived from the principle of conservation of energy applied at the surface of the imaged regions. A linear form of the model is used to derive features that remain constant despite changes in scene parameters/driving conditions. Simulated and real imagery, as well as ground truth thermo-couple measurements were used to test the behavior of such features. A method of change detection in outdoor scenes is investigated. The invariants are used to detect when a hypothesized material no longer exists at a given location. For example, one can detect when a patch of clay/gravel has been replaced with concrete at a given site. This formulation yields promising results, but it can produce large values outside a normally small range. Therefore, we adopt a new feature classification algorithm based on the theories of symmetric, alpha-stable (SαS) distributions.[14,15] We show that symmetric, alpha-stable distributions model the thermophysical invariant data much better than the Gaussian model and suggest a classifier with superior performance.

1 INTRODUCTION

Object recognition requires robust and stable features that are separable in feature space. An important characteristic of these features is that they be invariant to scene conditions, such as illumination, and changes in viewpoint/object pose. The formulation of invariant features, and the quantitative analysis of feature variance is currently being addressed by a number of researchers in the computer vision community, and has led to the establishment of a mature and growing theory of feature invariance.[1–4] However, such efforts have primarily considered reflected-light imagery – formed by sensing visible wavelength energy.

Non-visible modalities of sensing have been shown to greatly increase the amount of information that can be used for object recognition. A very popular and increasingly affordable sensor modality is thermal imaging - where non-visible radiation is sensed in the long-wave infrared (LWIR) spectrum of $8\mu m$ to $14\mu m$. The current generation of LWIR sensors produce images of contrast and resolution that compare favorably with broadcast television quality visible light imagery. However, the images are no longer functions of only surface reflectance. As the wavelength of the sensor transducer passband increases, emissive effects begin to emerge as the dominant mode of electromagnetic energy exitance from object surfaces. The (primarily) emitted radiosity of LWIR energy

*This research was supported by an ARPA RADIUS Technology Initiative seed contract from Lockheed-Martin, the AFOSR contract F49620-93-C-0063, the AFOSR grant LRIR-93WL001, an AFOSR Laboratory Graduate Fellowship, and ARPA contract F33615-94-C-1529.

has a strong dependence on internal composition, properties, and state of the object such as specific heat, density, volume, heat generation rate of internal sources, etc. This dependence may be exploited by specifying image-derived invariants that vary only if these parameters of the physical properties vary.

In this paper we describe the use of the principle of conservation of energy at the surface of the imaged object to specify a functional relationship between the object's thermophysical properties (e.g., thermal conductivity, thermal capacitance, emissivity, etc.), scene parameters (e.g., wind temperature, wind speed, solar insolation), and the sensed LWIR image gray level. We use this functional form to derive invariant features that remain constant despite changes in scene parameters/driving conditions. In this formulation the internal thermophysical properties play a role that is analogous to the role of parameters of the conics, lines and/or points that are used for specifying geometric invariants when analyzing visible wavelength imagery. Thus, in addition to the currently available techniques of formulating features that depend only on external shape and surface reflectance discontinuities, the phenomenology of LWIR image generation can be used to establish new features that "uncover" the composition and thermal state of the object, and which do not depend on surface reflectance characteristics.

The derivation of thermophysical invariants (TI's) from non-visible wavelength imagery, the evaluation of the performance of these invariants, and their use in object recognition systems poses several advantages. The main advantage of this approach is the potential availability of a number of new (functionally independent) invariants that depend on internal compositional properties of the imaged objects. Note that it is possible to evaluate the behavior of thermophysical invariants using ground truth data consisting of images of objects of known composition and internal state. This additional information can be used to augment/complement the behavior of Geometric Invariants (GI's).

Automatic site change detection has many important applications in the area of computer vision and image understanding. In one example of such a task, images are obtained, periodically, by an aircraft or satellite flying over a site to be monitored. The imagery is compared with known prior information or detailed site models to determine if any changes have occurred. For example, it may be important to detect if a patch of gravel or dirt has been replaced with a concrete or asphalt surface at some factory or construction site being monitored. Since some information is usually available of the site being monitored (in the form of site models), and also of the imaging parameters of the sensors, the site change detection task follows the paradigms of context-based vision and model-based vision. It is also closely related to the task of object recognition where a hypothesis of an object composed of different material types is verified or refuted. A particular site may be considered to be a composition of a specific collection of materials. A feature may be used to verify the existence of this composition. A change in the site should result in a feature value other than that expected for the original site. Change detection by this method may be used as a cue to direct detailed interpretation by a human operator.

The ideas presented in this paper are continuations/extensions of previous and ongoing research in thermophysical model-based interpretation of LWIR imagery. A brief description of this thermophysical approach is presented in section 2, followed by the formulation of a method to derive thermophysical invariants in section 3. Preliminary experimental results of applying this new approach to real imagery are presented in section 4, which is followed by a discussion of the behavior of the new method, issues to be considered in using this method for object recognition, and issues that remain to be explored.

2 A THERMOPHYSICAL APPROACH TO LWIR IMAGE ANALYSIS

A physics-based approach that attempts to establish features that depend only on thermophysical object properties has been reported.[6,7] A thermophysical model was formulated to allow integrated analysis of thermal and visual imagery of outdoor scenes. Although the approach is powerful in that it makes available features that are completely defined by internal object properties, the thermophysical feature estimates were not sufficiently reliable due to errors in segmentation and registration of the thermal and visual image pairs, and the noise-sensitivity of shape-from-shading techniques used in computing relative orientation of the surface.[8] A statistically robust scheme for computing the thermophysical feature R was proposed to minimize this drawback.[9] However, the computational complexity for such a technique is very high. Another limitation in the previous formulation is that a low Biot number was assumed, viz., the surface was assumed to be a thin plate, which is rarely satisfied in practise. Also, the technique requires *a priori* knowledge of several surface and scene parameters such as

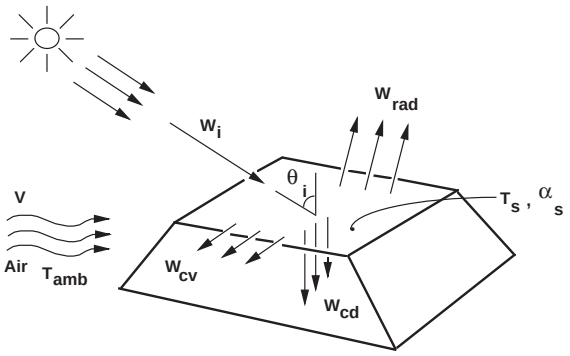

Figure 1: Energy exchange at the surface of the imaged object. Incident energy is primarily in the visible spectrum. Surfaces loses energy by convection to air, via radiation to the atmosphere, and via conduction to the interior of the object. The elemental volume at the surface also stores a portion of the absorbed energy.

emissivity, wind speed, solar insolation, etc, which in many applications are unavailable. Even in those situations where such information is available, the thermophysical feature, R, is only weakly invariant. While separation between classes is preserved, the range of values of R for each class is observed to vary with time of day and season of year. Also, the feature R is able to only separate very broad categories of objects, such as automobiles, buildings, and vegetation - it lacks the specificity to differentiate between different models of vehicles.

An improved formulation for establishing thermophysical features is described in this paper, wherein the features are computed only from a single LWIR image of a scene. Moreover, the technique does not require *a priori* knowledge of the many surface and scene parameters mentioned above. We present, at first, the thermophysical model based on the conservation of energy at the surface of the imaged object. This is followed by the derivation of the invariant feature using algebraic invariance theory, in section 3.

At the surface of the imaged object (figure 1) energy absorbed by the surface equals the energy lost to the environment.

$$W_{abs} = W_{lost} \tag{1}$$

Energy absorbed by the surface is is given by

$$W_{abs} \;=\; W_I \; cos\theta_I \; \alpha_s \;, \tag{2}$$

where, W_I is the incident solar irradiation on a horizontal surface, θ_i is the angle between the direction of irradiation and the surface normal, and α_s is the surface absorptivity which is related to the visual reflectance ρ_s by $\alpha_s = 1 - \rho_s$. Note that it is reasonable to use the visual reflectance to estimate the energy absorbed by the surface since approximately 90% of the energy in solar irradiation lies in the visible wavelengths.[10]

The energy lost by the surface to the environment was given by

$$W_{lost} \;=\; W_{cv} \;+\; W_{rad} \;+\; W_{cnd} \;+\; W_{st} \tag{3}$$

The energy convected from the surface to the ambient air is given by $W_{cv} \;=\; h(T_s \;-\; T_{amb})$ where, T_{amb} is the ambient air temperature, T_s is the surface temperature of the imaged object, and h is the average convected heat transfer coefficient for the imaged surface, which depends on the wind speed, thermophysical properties of the air, and surface geometry.[10] We note that surface temperature may be estimated from the thermal image based on an appropriate model of radiation energy exchange between the surface and the infrared camera.

The radiation energy loss is computed from $W_{rad} \;=\; \epsilon\;\sigma\;(T_s^4 - T_{amb}^4)$, where σ denotes the Stefan-Boltzman constant. The energy conducted to the interior of the object is given by $W_{cnd} \;=\; -k\;dT/dx$, where k is the thermal conductivity of the material, and x is distance below the surface. Here, we assume that lateral energy conduction is insignificant compared to conduction along the direction normal to the surface. The increase in the stored, internal energy of an elemental volume at the surface is given by $W_{st} \;=\; C_T \frac{dT_s}{dt}$, where C_T denotes the lumped thermal capacitance of the object and is given by $C_T = DVc$, D is the density of the object, V is the volume, and c is the specific heat. Considering a unit area on the surface of the imaged object, the equivalent

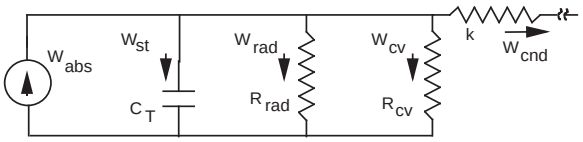

Figure 2: The equivalent thermal circuit for the extended model that separates the stored energy component and the conduction component to the interior of the object.

thermal circuit for the surface is shown in figure 2. The resistances are given by: $R_{cv} = 1/h$, $R_{cnd} = 1/k$, and $R_{rad} = 1/(\epsilon\sigma(T_s^2 + T_{amb}^2)(T_s + T_{amb}))$

In the following section we use the energy conservation model described above to derive invariant features using ideas in algebraic invariance theory.[11]

3 THERMOPHYSICAL ALGEBRAIC INVARIANTS

The energy balance equation, $W_{abs} = W_{rad} + W_{cv} + W_{st} + W_{cnd}$ may be rewritten in the following linear form:

$$a^1 x_1 + a^2 x_2 + a^3 x_3 + a^4 x_4 + a^5 x_5 = 0. \tag{4}$$

Using the expressions for the various energy components as presented in section 2 we can express each term in the above expression as:

$$\begin{array}{ll} a^1 = cos\theta_I & x_1 = W_I \alpha_s \\ a^2 = -\sigma\ (T_s^4 - T_{amb}^4) & x_2 = \epsilon \\ a^3 = -(T_s - T_{amb}) & x_3 = h \\ a^4 = C_T & x_4 = -\frac{dT_s}{dt} \\ a^5 = kT_s & x_5 = 1 - \frac{T_{int}}{T_s} \end{array} \tag{5}$$

The term $a^5 x_5$ denotes W_{cnd} expressed in a finite difference form.

Note that a calibrated LWIR image provides radiometric temperature. Hence a^2 and a^3 can be computed from the LWIR image alone (and knowledge of the ambient temperature), while a^1 and a^4 are known when the identity and pose of the object is hypothesized, and a^5 is computed using the image and the hypothesis. The "driving conditions", or unknown scene parameters[1] that change from scene to scene are given by the x_i. For each pixel in the thermal image eqn (5) defines a hyperplane in 5-D space.

3.1 An algebraic invariance formulation

Consider two different LWIR images of a scene obtained under different scene conditions and from different viewpoints. Consider N points on the object that (a) are visible in both views, and (b) have been selected to lie on different components of the object which differ in material composition and/or surface normal direction. Assume (for the nonce) that the object pose for each view, and point correspondence between the two views are available (or hypothesized). A point in each view yields a contravariant tensor a^i as defined by eqn (5). Let the collection of these tensors be denoted by $a_k^i, k = 1, 2, \ldots, N$ for the first scene/image and $b_k^i, k = 1, 2, \ldots, N$ for the second scene. For the k-th point we denote the measurement tensor as $\mathbf{a_k}$ for the first view, and as $\mathbf{b_k}$ for the second view, and the driving conditions tensor as $\mathbf{x^k}$.

We assume that the scene/driving conditions, $\mathbf{x^k}$ for the first view and $\mathbf{y^k}$ for the second view, are related by an affine transformation. The justification of this assumption is discussed below. We have found, empirically, that this assumption holds when the points are selected using the method discussed later in this paper. Since the $\mathbf{x^k}$ are transformed affinely, then it follows that the $\mathbf{a_k}$ are also transformed affinely. Note that an affine transformation from one scene to another is trivial to obtain if we have only five points that generate five non-

[1] Here, we use the Einstein notation to denote the image-based measurement vector as a contravariant tensor,a^i, while the changing scene conditions form a covariant tensor,x_i. Therefore, $a^i x_i = 0$.

coplanar tensors in our 5-D measurement space. Consider one such subset of 5 of the N points, and denote them as i, j, l, m, and n.

The determinant

$$d(\mathbf{a_i a_j a_l a_m a_n}) = \begin{vmatrix} a_i^1 & a_i^2 & a_i^3 & a_i^4 & a_i^5 \\ a_j^1 & a_j^2 & a_j^3 & a_j^4 & a_j^5 \\ a_l^1 & a_l^2 & a_l^3 & a_l^4 & a_l^5 \\ a_m^1 & a_m^2 & a_m^3 & a_m^4 & a_m^5 \\ a_n^1 & a_n^2 & a_n^3 & a_n^4 & a_n^5 \end{vmatrix} \tag{6}$$

defines the "volume" of the oriented parallelepiped formed by the pencil of the five contravariant tensors $\mathbf{a_i}, \mathbf{a_j}, \mathbf{a_l}, \mathbf{a_m}, \mathbf{a_n}$. The above determinant is a relative invariant to the affine transformation,[11] i.e.,

$$d(\mathbf{a_i a_j a_l a_m a_n}) = \delta_{ijlmn} \times d(\mathbf{b_i b_j b_l b_m b_n}) \tag{7}$$

where δ_{ijlmn} is the determinant of the affine transformation, T_{ijlmn}, which relates the measurement tensors, i.e., $\mathbf{a_k} = \mathbf{b_k} T_{ijlmn}$, $k \in \{i, j, l, m, n\}$.

Consider another set of five points in which at least one point is different from the previous set. Denote this second set as $\{p, q, r, s, t\}$. Again, assume that the measurement tensors for this collection of points undergo an affine transformation from the first scene to the second, and denote this transformation by T_{pqrst}.

$$d(\mathbf{a_p a_q a_r a_s a_t}) = \delta_{pqrst} \times d(\mathbf{b_p b_q b_r b_s b_t}) \tag{8}$$

where $\delta_{pqrst} = \det(T_{pqrst})$. Hence, if $\delta_{ijlmn} = \delta_{pqrst}$, then we can define an absolute invariant as

$$I = \frac{d(\mathbf{a_i a_j a_l a_m a_n})}{d(\mathbf{a_p a_q a_r a_s a_t})} \tag{9}$$

Note that the existence of affine transformations T_{ijlmn} and T_{pqrst} is easy to ensure by selecting the points that lie on different material types and/or have different surface normals. However, the existence and selection of two sets of five points such that $\delta_{ijlmn} = \delta_{pqrst}$ holds is crucial to the existence and determination of an absolute invariant. Our experimental investigation shows that point sets that satisfy this equivalence class of transformations are plentiful on any real, complex object such as a vehicle. The thermophysical justification for the existence of this equivalence class will be addressed in our future work.

The selection of the two sets (with five points in each) that satisfy this equivalence relationship may be attempted as a data-driven training task as follows. Calibrated LWIR imagery from different object classes are obtained at different times of day and different seasons of the year. N points are picked on an object – on distinctive components that differ in material composition and/or surface normal. Consider the image from time t_u and the image from t_v, $u \neq v$. The measurements at t_u along with the hypothesis of the identity of the object form the tensors $\mathbf{a_k}$. Similarly, image information at time t_v is used to form the measurement tensors $\mathbf{b_k}$.

All combinations of two sets of five points each, $\{i, j, l, m, n\}$ and $\{p, q, r, s, t\}$, are examined. The measurement matrices $(\mathbf{a_i a_j a_l a_m a_n})$, $(\mathbf{b_i b_j b_l b_m b_n})$, $(\mathbf{a_p a_q a_r a_s a_t})$, and $(\mathbf{b_p b_q b_r b_s b_t})$ are constructed. The transformations T_{ijlmn} and T_{pqrst}, if they exist, and the their determinants δ_{ijlmn}, and δ_{pqrst} are computed. The two sets that best satisfy $\delta_{ijlmn} = \delta_{pqrst}$ for different choices of pairs of scenes/images, i.e. different choices of t_u and t_v, are selected. With N points, the number of possible choices of the pair of sets of points is given by

$$n_{_N} \;=\; \frac{1}{2} \left(\frac{N!}{(N-5)!5!} \right) \left(\frac{N!}{(N-5)!5!} - 1 \right) \tag{10}$$

In order for the invariant feature to be useful for object recognition the value of I must be different if the measurement vector is obtained from a scene that does not contained the hypothesized object and/or the hypothesized pose is incorrect. A search for the best sets of points that both identify the object and separate the classes must be conducted over the $n_{_N}$ point sets. The point sets may be rated for their intra-class invariance, then the best choices may be used to evaluate their inter-class separability.

3.2 Employing TAI's for object recognition / change detection

The feature computation scheme formulated above is suitable for use in an object recognition system that employs a hypothesize-and-verify strategy. The scheme would consist of the following steps: (1) extract geometric

(a) (b)

Figure 3: (a) Truck-type vehicle with points selected on the surface of different components with different material properties and/or surface normals. (b) Military Tank vehicle with points selected on the surface of different components with different material properties and/or surface normals.

features, e.g., lines and conics, (2) for image region, r, hypothesize object class, k, and pose using, for example, geometric invariants as proposed by Forsyth, et al,[2] (3) use the model of object k and project visible points labeled $i = 1, 2, \ldots$ onto image region r using scaled orthographic projection, (4) for point labeled i in the image region, assign thermophysical properties of point labeled i in the model of object k, (5) use the gray levels at each point and the assigned thermophysical properties, to compute the measurement matrices A and A', and hence compute the feature $f^k(r) = |A|/|A'|$, and finally, (6) compare feature $f^k(r)$ with model prototype $\hat{f_k}$ to verify the hypothesis.

The application of this scheme for site change detection is straightforward. For a site being monitored, M different types of surfaces are selected *a priori* to produce a thermophysical algebraic invariant. Note that we must have $M > 5$. One may also be able to specify more than one TAI, and hence establish a feature vector. When one or more of the surfaces change (e.g., from gravel to concrete) then the feature (vector) computed from the scene under the hypothesis of the prior material types will produce a value different from that expected. The detection of the change is thus linked to the refutation of an incorrect hypothesis.

4 EXPERIMENTAL RESULTS

The approach described in the previous section was evaluated using real and simulated data. The usefulness of the scheme for object recognition was tested using real LWIR imagery of two different vehicles at different times of the day. An exhaustive investigation of the behavior of features derived by the new method was studied using simulated data. The usefulness of the approach for site change detection was studied using ground truth temperature measurements obtained from thermocouples planted in various materials placed in an outdoor scene and also from LWIR images of an outdoor scene sensed at different times of the day.

4.1 Object recognition using real imagery

The method of computing thermophysical algebraic invariants discussed above was applied to real LWIR imagery acquired at different times of the day. Two types of vehicles were imaged: a military truck and a military tank (figure 3). Several points were selected, as indicated in the figure, on the surfaces of different materials and/or orientation. The measurement tensor given by eqn (5) was computed for each point, for each image/scene.

The method used to select optimal sets of points $\{i, j, l, m, n\}$ and $\{p, q, r, s, t\}$ was similar to that described in section 3 – however, instead of using the equivalence of the determinants of the two affine transformations as the selection criterion, we used the variance in the values of the feature computed for different scenes (i.e., images

Time of Day	Hypothesis: Truck Data from: Tank	Hypothesis: Truck Data from: Truck
11 am	.003	-.03
12 n	.01	-.01
1 pm	.01	-.02
2 pm	.01	-.01
3 pm	.001	-.01

Table 1: Inter-class variation vs. intra-class variation for set A consisting of point sets $\{2,3,4,6,7\}$ and $\{3,4,10,7,8\}$ for Truck vehicle. Thermophysical properties are chosen for a Truck vehicle hypothesis. The middle column shows feature values computed when the measurement tensors are obtained from a Tank vehicle.

Time of Day	Hypothesis: Tank Data from: Truck	Hypothesis: Tank Data from: Tank
11 am	-.001	0.4
12 n	-.01	0.7
1 pm	-.03	0.2
2 pm	-.002	0.4
3 pm	.05	0.4

Table 2: Inter-class variation vs. intra-class variation for point set B. Points and thermophysical properties are chosen for a Tank vehicle hypothesis. The middle column shows feature values computed when the measurement tensor is obtained from a Truck vehicle.

obtained at different times of day) containing the object.

Many different pairs of five-point-sets yielded features with low variance from scene to scene, but not all demonstrated good between-class separation. As mentioned in section 3 one must consider inter-class behavior as well as intra-class behavior during feature selection. To investigate this we adopted the following procedure. Given an image of a vehicle, (1) assume the pose of the vehicle is known, then (2) use the front and rear wheels to establish an object centered reference frame. The center of the wheel is used as the origin, and center of the front wheel is used to specify the direction and scaling of the axes. The coordinates of the selected points are expressed in terms of this 2D object centered frame. Thus when the truck vehicle type is hypothesized for an image that is actually obtained of the tank or some unknown vehicle, the material properties of the truck are used, but image measurements are obtained from the image of the observed vehicle at locations given by transforming the coordinates of the truck points (in the truck centered coordinate frame) to the image frame computed for the unknown vehicle.

Table 1 shows inter-class and intra-class variation when the truck vehicle is hypothesized, and for images obtained at five different times in the day. Table 2 shows inter-class and intra-class variation when the tank vehicle is hypothesized. Such investigation showed that some selection of points produced almost identical values irrespective of the source of the measurements. These sets have good (low) intra-class variation but poor inter-class separation, and they do not distinguish the truck vehicle from the tank vehicle. Sets A and B, however, can be seen to demonstrate good inter-class separation and acceptable intra-class invariance.

4.2 Sensitivity analysis using simulated data

In order to investigate the robustness of the thermophysical features derived above, the sensitivity of the features to object and scene parameter variations were evaluated.[12] Examination of feature variation was based on simulating the various scene and object energy components for varying scene parameter values - and predicting the feature value. These simulations were performed on thermophysical object models that were based on equivalent thermal circuits. A widely available circuit simulator was used to implement these circuits. The model was then used to investigate the intra-class invariance and inter-class separability of the features with respect to the following

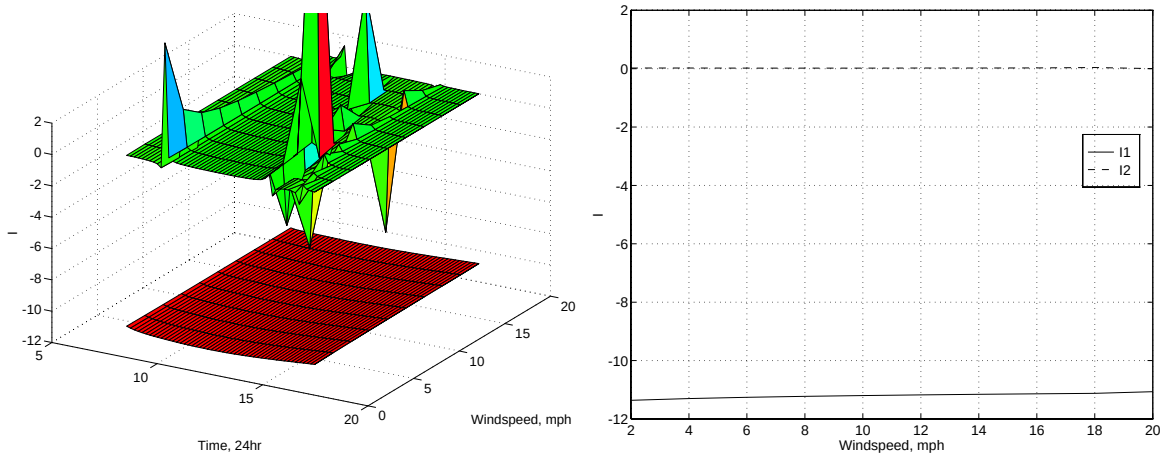

(a) (b)

Figure 4: (a) Variation of features A and C with wind speed over the period of an entire day. Feature C is computed from the point sets $\{1,3,4,6,7\}$ and $\{2,3,6,7,8\}$ for the Truck vehicle. (b) Variation of features A and C with windspeed at 12 noon.

parameters: (1) time of day, (2) day of year, (3) wind speed, (4) object pose, (5) surface absorptivity, and (6) assumed and actual surface emissivity. This approach eliminates the expensive and impractical task of collecting real imagery under all possible scene conditions. The values of the features themselves closely corresponded to values calculated from real data when available. An example of the behavior of the features during parameter variation is shown in figure 4. In this case the wind speed has been varied from 2 to 20 MPH. Note that feature A contains singularities. The singularities occur when the temperature vs time curves of different points in the scene cross each other. These singularities are highly localized in time, and the two features continue to be well separated. Similar results have been obtained with respect to the variation of the other parameters for each of the features discussed above.

4.3 Site change detection

The usefulness of these thermophysical invariant features for site change detection tasks was examined, experimentally, by analyzing "ground truth" data gathered from a scene. The data consisted of temperature measurements acquired from thermocouples implanted in various types of materials placed in an outdoor scene. The data were collected over a period of five days in mid-November. The collection includes varying weather conditions and has extensive records of the atmospheric pressure, ambient temperature, lighting conditions, etc. The measurements were recorded at closely spaced intervals of a few minutes. The materials included sod, clay, gravel, concrete, asphalt, and aluminum. Extensive modeling of the test site has been done, and simulations have reproduced the actual data to within $0.5^{o}C$.

Consider a feature constructed (as described in section 3) using point sets {Grass, Clay, Gravel, Asphalt, Aluminum} and {Grass, Clay, Concrete, Asphalt, Aluminum}. The distribution of the value of this feature was computed when the measurements were obtained from the correctly hypothesized materials. The average value of the feature was -91.4, and the standard deviation was 1.7. Next, measurements for one of the hypothesized materials was obtained from a different material – to mimic the situation where one of the materials in the site is changed to a different one. The mean and standard deviation were computed for the feature value under this erroneous hypothesis. For change detection we should notice a significant difference in feature values computed under correct and wrong hypotheses. The feature's behavior under different wrong hypotheses is summarized in table 3.

Four different features, $\{x, y, z, w\}$, were constructed, and their behavior under correct and wrong hypotheses

Data from	Hypothesized Material					
	Grass	Clay	Gravel	Concrete	Asphalt	Aluminum
Grass	-91.4,1.7	-91.2, 1.6	-91.1, 2.0	-91.5, 2.3	-90.0,6.2	-92.0, 5.3
Clay	-72.8, 40.2	-91.4, 1.7	-72.9, 40.2	-91.7, 3.4	-74.4, 42.7	-80.0, 6.1
Gravel	-73.6, 40.8	-70.1, 39.3	-91.4, 1.7	-91.1, 0.1	16.4, 38.8	-84.0, 5.1
Concrete	-89.9, 0.8	-89.7, 0.4	-91.0, 0.1	-91.4, 1.7	-110.4, 0.1	-98.5, 6.2
Asphalt	-56.4, 31.8	-108.9, 90.3	17.8, 50.1	-110.1,3.9	-91.4,1.7	-87.9, 7.5
Aluminum	-90.9, 1.7	-91.0, 1.6	-91.2, 1.6	-91.1, 1.6	-91.6, 1.5	-91.4, 1.7

Table 3: The (mean, standard deviation) values for a feature constructed using point sets {Grass, Clay, Gravel, Asphalt, Aluminum} and {Grass, Clay, Concrete, Asphalt, Aluminum}. The values of this feature were computed when the measurements were obtained from the correctly hypothesized materials and also for specific erroneous hypotheses.

Data from	Hypothesized Material					
	Grass	Clay	Gravel	Concrete	Asphalt	Aluminum
Grass		0.11	0.10	0.11	0.11	0.38
Clay	0.01		0.01	0.32	0.00	0.21
Gravel	0.01	0.01		0.19	0.01	0.16
Concrete	0.08	0.08	0.19		0.00	0.22
Asphalt	0.06	0.06	0.02	0.05		0.06
Aluminum	0.49	0.50	0.50	0.50	0.50	

Table 4: Bhattacharya upper bound on the probability of error, i.e., missed detection of a change, using four invariant features.

was examined. The distribution of a feature, x, under the correct hypothesis was modeled as a Gaussian pdf, $p_1(x)$, and its distribution under a specific erroneous hypothesis was modeled as another Gaussian pdf, $p_2(x)$. The ability of the feature to separate these two cases may be measured by the *Bhattacharya bound* on the error probability[13] given by

$$\epsilon_u = \sqrt{P_1 P_2} e^{-\mu(1/2)} \tag{11}$$

where the prior class probabilities P_1, P_2 may be assumed to be equal,

$$\mu(1/2) = \frac{1}{8}(m_2 - m_1)^T \left(\frac{\Sigma_1 + \Sigma_2}{2}\right)^{-1} (m_2 - m_1) + \frac{1}{2} \ln \frac{\left\| \frac{\Sigma_1 + \Sigma_2}{2} \right\|}{\sqrt{|\Sigma_1||\Sigma_2|}} \tag{12}$$

and Σ_1, Σ_2 and m_1, m_2 are the class covariance and the mean, respectively. Note that the Bhattacharya bound does not use the optimal classifier, and is hence a loose upper bound. Also, we adopt univariate distributions to model each feature under each hypothesis. We select the lowest error bound for detecting a particular change in material type. These error bounds are indicated in table 4. It is evident that even with a small number of features, change detection is possible with a low probability of missed detection. We expect that with additional features the actual error probabilities (as opposed to the upper bound) can be further reduced to a much lower level.

Unfortunately, as we increased the number of data points considered, the variance of the thermo-physical invariant increased rapidly. We also noted that the variance did not appear to converge. This is a clear indication that the thermo-physical invariants do not fit a Gaussian model. A more appropriate model and a new classification scheme are required.

Symmetric, Alpha-Stable (SαS) processes form a class of statistical models with several interesting properties, one of which is the lack of finite statistics of order higher than the corresponding characteristic exponent. SαS processes have been receiving increasing interest from the signal processing and communications communities in the very recent years as statistical-physical models for time series containing severe outliers.[14] The performance of Gaussian classifiers on such observations is unacceptably low. However, significant performance gains can be obtained if proper, non-Gaussian classifiers are developed.

(a) (b)

Figure 5: (a) A visual image of the scene used for these experiments. Materials include Asphalt, Concrete, Dirt, Fiberglass, Iron, Slate, and Wood. (b) A corresponding long-wave infrared (LWIR) image.

A univariate SαS pdf $f_\alpha(\gamma, \delta; \cdot)$ is best defined via the inverse Fourier transform integral[14]

$$f_\alpha(\gamma, \delta; x) = \frac{1}{2\pi} \int_{-\infty}^{\infty} \exp(i\delta\omega - \gamma|\omega|^\alpha) e^{-i\omega x}\, d\omega \tag{13}$$

and is completely characterized by the three parameters α (*characteristic exponent*, $0 < \alpha \leq 2$), γ (*dispersion*, $\gamma > 0$), and δ (*location parameter*, $-\infty < \delta < \infty$).

The characteristic exponent α relates directly to the heaviness of the tails of the SαS pdf. The smaller its value, the heavier the tails. The value $\alpha = 2$ corresponds to a Gaussian pdf, while the value $\alpha = 1$ corresponds to a Cauchy pdf. The dispersion γ is a measure of the spread of the pdf, similar to the variance of a Gaussian pdf. Finally, the location parameter, δ, is the point of symmetry of the pdf and equals its mean, whenever the mean is finite (i.e., for $1 < \alpha \leq 2$).

The non–Gaussian ($\alpha \neq 2$) SαS distributions maintain many similarities to the Gaussian distribution, but at the same time differ from it in some significant ways. For example, a non–Gaussian SαS pdf maintains the usual bell shape and, more importantly, non–Gaussian SαS random variables satisfy the linear stability property. However, non–Gaussian SαS pdfs have much sharper peaks and much heavier tails than the Gaussian pdf. As a result, only their moments of order $p < \alpha$ are finite, in contrast with the Gaussian pdf which has finite moments of arbitrary order. These and other similarities and differences between Gaussian and non–Gaussian SαS pdfs and their implications on the design of signal processing algorithms are presented in detail in the tutorial paper[15] or in the recent monograph[14] to which the interested reader is referred.

We selected a particular thermophysical invariant that showed promise as a good feature for site change detection. We tested this invariant on our site change IR imagery. Figure 6(a) illustrates that the amplitude probability distribution of the feature and the alpha-stable model agree very well. Note that a typical estimate of the variance of these features is 10^5, which is a clear indication of infinite variance.[14] Figure 6(b) shows that the feature distribution under an incorrect hypothesis can also be modeled by a SαS distribution. This clearly indicates that classifiers based on SαS processes will perform better than conventional classifiers designed under the Gaussian assumption.

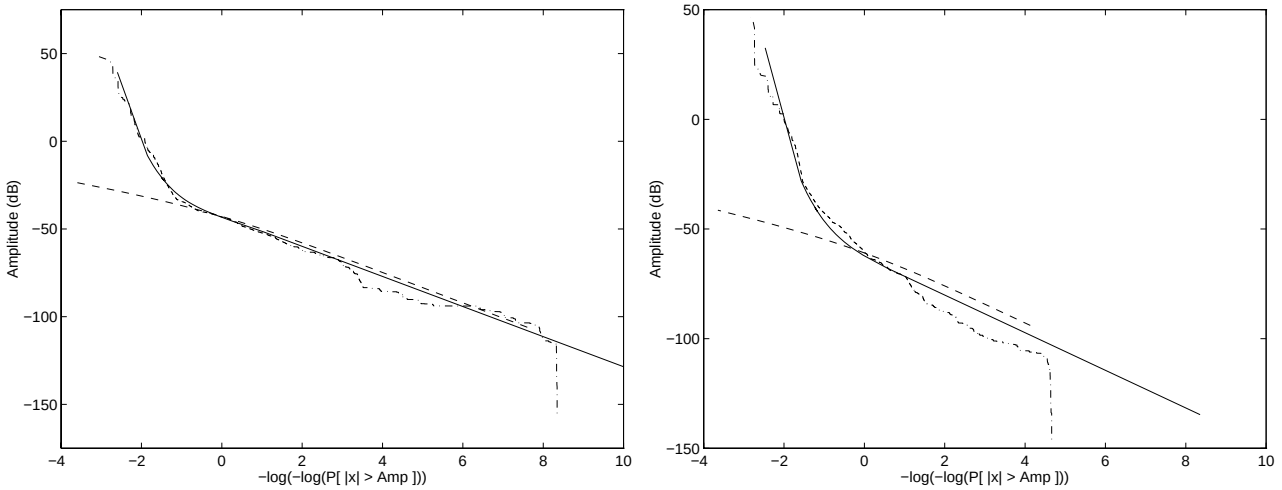

Figure 6: (a) Theoretical SαS Amplitude Probability Distribution (APD) with $\alpha = 1.3$ and $\gamma = 0.001$ ($\delta = 0.1325$) matches the correct hypothesis data very well. The dashed line is the best Gaussian (hand-fitted $\sigma = .008$) approximation. Notice that in the tail region (The upper-left curved part) the Gaussian model diverges from the data. (b) An incorrect hypothesis can also be modeled very well ($\alpha = 0.8$, $\gamma = 0.0075$, and $\delta = 0.0095$, Gaussian $\sigma = .001$).

5 DISCUSSION

The approach described above is promising in that it makes available features that are (1) invariant to scene conditions, (2) able to separate different classes of objects, and (3) based on physics based models of the many phenomena that affect LWIR image generation.

The specification of optimal sets of points for high inter-class separation and low intra-class variation is a crucial task in this approach. This is a complex search problem, and it is not clear that a solution will always exist for a collection of object classes. Some criteria for the choice of point sets are obvious. Points should not be chosen such that the measurement matrix has less than full rank. This occurs, for example, when the five points lie on surfaces with identical surface normals and identical thermophysical properties.

When the two sets of points have four points in common, and when the remaining two points are on different parts of the imaged object, but lie on materials that are identical/similar, then these points will form an invariant that has magnitude of one. Such invariants are useful only if there exists a unique set, or limited number of sets, of points that produces this value. Other thermophysical criteria for point set selection need to be investigated.

Considering a simple case of the point set selection gives insight into the formulation of the invariant feature. Recall that two sets of five points are required to form the feature value. The simplest method to form two sets is to replace one point in the first set with a distinct point in the second set. For a given scene we may construct: $A = [\mathbf{a_1 a_2 a_3 a_4 a_5}]$ and $A' = [\mathbf{a_1 a_2 a_3 a_4 a_6}]$, the measurement matrices with measurement tensors, $\mathbf{a}$'s, as defined in section 3. Consider $\vec{n}$, which spans the null space of $A^* = [\mathbf{a_1 a_2 a_3 a_4}]$, i.e. $A^*\vec{n} = 0$. The feature value, $\frac{|A|}{|A'|}$, is non-zero if and only if $\mathbf{a}_5^T \cdot \vec{n} \neq 0$ and $\mathbf{a}_6^T \cdot \vec{n} \neq 0$. Furthermore, it can be shown that:

$$\frac{|A|}{|A'|} = \frac{\mathbf{a}_5 \cdot \vec{n}}{\mathbf{a}_6 \cdot \vec{n}} \tag{14}$$

A topic of future research is to find $\vec{n}$ such that it varies little from scene to scene. If such a formulation can be found it will be possible to pre-compute $\vec{n}$ for a given object. This will reduce the required measurements in the image to two points.

There remain many issues that require further research. First, a thermophysical justification is required for the

measurement tensors have identical determinants for any two scenes. A linear form of the energy balance model, eqn. 4, that is not homogeneous could be developed. This would reduce the dimensionality of the measurement vector, and depending on the choice of terms – eliminate the requirements for hypothesis of pose and hypothesis of specific thermophysical parameter values, but at the risk of impaired invariance and separability. It would be useful to integrate the above scheme with GI's that could hypothesizes pose and identity, which would then be verified by the scheme described in this paper. A detailed exploration of the performance of the scheme when applied to a significant collection of objects, aspects, and scene conditions is also required.

6 REFERENCES

[1] T.H. Reiss, "Recognizing Planar Objects Using Invariant Image Features", *Lecture Notes in Computer Science, 676,* G. Goos and J. Hartmanis (Eds), Springer-Verlag, Berlin, 1993.

[2] D. Forsyth, J.L. Mundy, A. Zisserman, C. Coelho, A. Heller, C. Rothwell, "Invariant Descriptors for 3D Object Recognition and Pose", *IEEE Trans PAMI*, vol 13, no 12, Oct 1991

[3] D. Weinshall, "Direct Computation of Qualitative 3D Shape and Motion Invariants", *IEEE Trans PAMI*, vol 13, no 12, Dec 1991.

[4] E. Rivlin and I. Weiss, "Semi-Local Invariants", *IEEE Trans PAMI*, March 1995.

[5] M.J. Gauder, V.J. Velten, L.A. Westerkamp, J. Mundy, and D. Forsyth, "Thermal Invariants for Infrared Target Recognition", *ATR Systems and Technology Conf*, 1993.

[6] N. Nandhakumar and J.K. Aggarwal, "Integrated Analysis of Thermal and Visual Images for Scene Interpretation", *IEEE Trans. on Pattern Analysis and Machine Intelligence*, Vol. 10, No. 4, July 1988, pp. 469-481.

[7] N. Nandhakumar, "A Phenomenological Approach to Multisource Data Integration: Analyzing Infrared and Visible Data", *Proc. IAPR TC7 Workshop on Multisource Data Integration in Remote Sensing,* College Park, MD, June 14-15, 1990.

[8] R. Zhang, P.-S. Tsai, J.E. Cryer, M. Shah, "Analysis of Shape from Shading Techniques", *Proc IEEE CVPR*, Seattle, WA, 1994, pp. 377-384.

[9] N. Nandhakumar, "Robust Physics-based Sensor Fusion", Journal of the Optical Society of America, JOSA-A, vol. 11, no. 11, Nov 1994, pp. 2981-2989

[10] F.P. Incropera and D.P. DeWitt, *Fundamentals of Heat Transfer*, John Wiley and Sons, New York, 1981.

[11] G.B. Gurevich, "Foundations of the Theory of Algebraic Invariants", (translated by J.R.M. Raddock and A.J.M. Spencer) P. Noordhoff Ltd - Groningen, The Netherlands, 1964

[12] G. Hoekstra and N. Nandhakumar, "Quasi-Invariant Behavior of Thermophysical Features for Interpretation of Radiometric Imagery", *Optical Engineering* to appear.

[13] K. Fukunaga, *Introduction to Statistical Pattern Recognition*, Academic Press, San Diego, CA, 1990

[14] C.L. Nikias and M. Shao, *Signal Processing with Alpha-Stable Distributions*, John Wiley and Sons, New York, 1995.

[15] M. Shao and C.L. Nikias, "Signal Processing with fractional lower-order moments: Stable processes and their applications", *Proc IEEE*, vol 81, pp 986-1010, 1993